A246: High Resolution Laser Spectroscopy Lab Report

Team A5

Aarathi Parameswaran

Purbita Kole

3rd August 2023

Bonn-Cologne Graduate School of Physics and Astronomy

University of Bonn

Advanced Lab Course

Winter Semester 2023/2024

Contents

1 Introduction

The aim of this lab is to use high-resolution laser spectroscopy using a single-mode extended cavity diode laser emitting radiation at 794 nm coupled to a Fabry-Perot Interferometer and is used to study the diode laser characteristics and perform spectroscopic techniques on Rubidium vapour and investigating the hyperfine structure.
The experiment consists mainly of three parts:

- The first part involves studying the diode laser characteristics and using the Fabry-Perot interferometer for frequency calibration and calculation of finesse.
- In the second part, linear spectroscopy technique is used to observe the D1 transition of Rubidium isotopes, considering the Doppler effects and measuring other parameters involved, including Doppler width, hyperfine coupling constants and isotope shift and verifying Lambert-Beer law.
- The third part uses a nonlinear spectroscopic technique to measure spectral lines with more accuracy without Doppler effects.

This report consists of a description of the experimental procedure and the analysis performed. [1]

2 Experimental Setup and Analysis

2.1 Diode Laser Characteristics

The diode laser used in the Rb spectroscopy,is characterised. The output power of the laser is measured corresponding to the change in injection current. From the characteristics parameters like Threshold Current, quantum efficiency of laser are derived

2.1.1 Experimental Setup

In this experiment a commercial diode laser ((Model DLC DL Pro from Toptica) is used which operates at mW range at $\lambda = 794$nm. The laser output is controlled by modulating the temperature and injection current.The diode laser is equipped with a laser controller as seen in Fig(1). The in-built scanning of this controller is not used for this part of the experiment. The temperature of laser was set to a fixed temperature above 20^oC. Only the injection current was varied while 'SCAN' and 'FEED-FORWARD' settings were switched off. The laser power is measured using a calibrated photodiode.The photodiode being at-

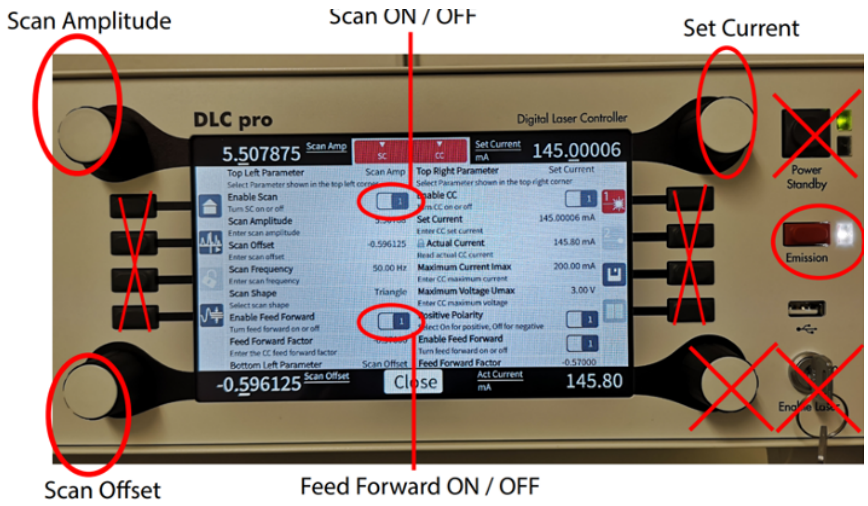

Figure 1: Display window of the laser control [1]

tached to a power-meter measuring the output in μW.To prevent the photodiode(saturation power $\approx 1.5mW$ from saturating a series of attenuators were used.The attenuators used for this measurement had $T(\text{Transmission}) = 0.105, 0.512$

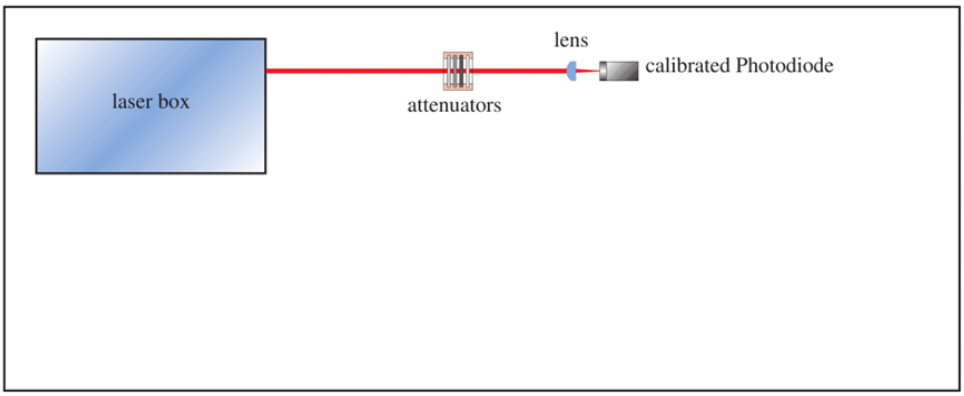

Figure 2: Optical Setup for Measuring the Laser Power.[1]

2.1.2 Measuring the laser characteristic graph

Measurement of laser power was done by varying the injection current between 0 to 120 mA.. At around **47 mA** there was a sharp increase in output power from zero.After lasing initiation,i.e for $I \in [47, 120]$mA the Power vs Injection current graph (Fig(3)) was fitted with a linear curve. The $I_{threshold}$ agrees with the fit value of $\mathbf{I}_{threshold}$**(threshold current)** of **47.75±0.01mA**.

From the fit in Fig(3), the slope-

$$\frac{dP_{out}}{dI} = \mathbf{0.4081 \pm 0.000005V} \tag{1}$$

The Quantum Efficiency of the laser is calculated as-

$$\sigma_{eff} = \frac{dP_{out}}{dI}\frac{e\lambda}{hc} = (\mathbf{26.1624 \pm 0.00086})\% \tag{2}$$

This value of efficiency is quite reasonable for commercial diode laser operating at visible wavelength.

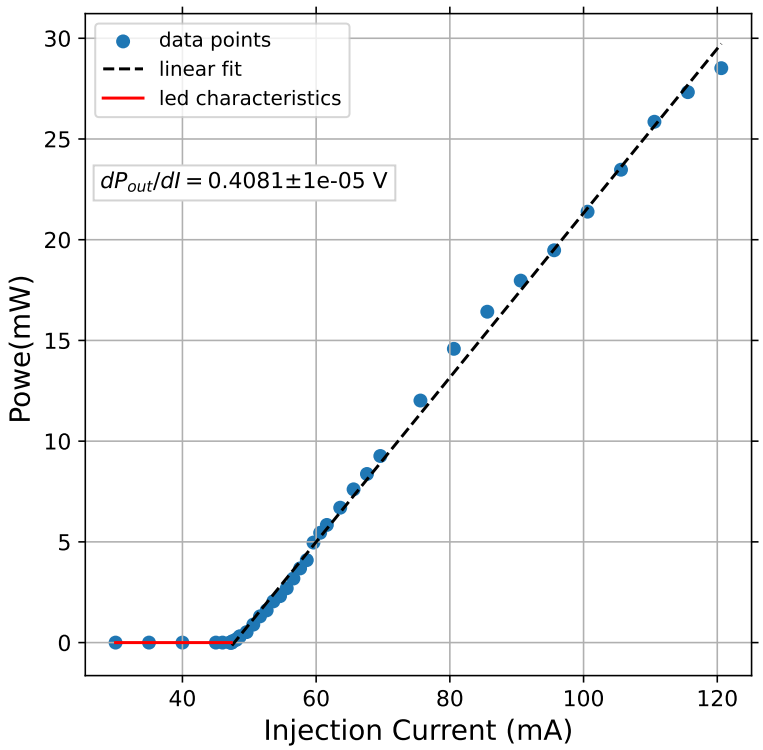

Figure 3: Diode Laser Characteristic Curve.

2.2 Calibration using Fabry–Pérot interferometer cavity

Fabry–Pérot interferometer cavity is used to calibrate the scanning laser signal passing through the Rb cell.In this experiment a confocal Farby Perot interferometer(**FPI**)is used. The specifications for the FPI are [1]

- Radius of curvature=500mm
- Length between two mirrors=500mm
- Reflectivity (R)=0.85 [1]

The periodic resonant transmission peaks are given by

$$T_{FPI} = \frac{1}{1 = Fsin^2\frac{\Phi}{2}} \tag{3}$$

[1]The reflectivity value is taken at λ =794nm which is the target wavelenth for Rb spectroscopy

with

$$F = \frac{4R}{(1-R)^2} \tag{4}$$

where Φ is the phase attained during one-round trip.In Free Spectral Range operation, transmission peaks are equally spaced and the spacing is given by-

$$\Delta\nu_{FSR} = \frac{c}{2nl} \tag{5}$$

In this experiment l(optical length)=500mm,n(R.I of air)=1 and the c(speed of light in air)is $\approx 2.99.10^8 \mathrm{ms}^{-1}$ .Using these values in Eq(5) -

$$\Delta\nu_{FSR} \approx 299\mathrm{MHz} \tag{6}$$

But the actual mode spacing between two transmission curves is given by-

$$\Delta\nu_{mode} = \frac{\Delta\nu_{FSR}}{2} = 149.5Mhz \tag{7}$$

For an ideal FPI and optimised coupling this value should remain constant.[2] This value was also calibrated prior to this experiment at$\Delta\nu_{mode}$=149.9348(2)MHz.[1] Here considering the mirrors to be highly reflective,finesse of the mirror is given by

$$\mathcal{F} = \frac{\pi\sqrt{R}}{1-R} \tag{8}$$

with R=0.85 the value is calculated to be $\mathcal{F} = \mathbf{19.309}$. From these values the FWHM of transmission curves are predicted by

$$\delta\nu_{FWHM} = \frac{\Delta\nu_{FSR}}{\mathcal{F}} = 7.76\mathrm{MHz} \tag{9}$$

2.2.1 Experimental Setup

For this part of the experiment, the scanning mode of the laser controller is switched on and the injected current is adjusted to "Feed Forward "settings. The scanning is done with a saw -tooth signal with a frequency of **15KHz**. Injection current was set at **162 mA** with a fixed scanning amplitude and offset.The signal for the etalon is send to an oscilloscope through a photodiode.The scanning ramp from the laser controller is also fed to the oscilloscope.The setup is as shown in Fig(4). The weak beam passing through a pinhole is used, to avoid reflections from FPI travelling back to the laser.In the oscilloscope the transmission signal is adjusted along the rising ramp of the saw-tooth signal(Fig(5).It is also seen that there is no mode hops in this signal, which indicates proper coupling of laser beam into the FPI and any absence of drift in the signal.

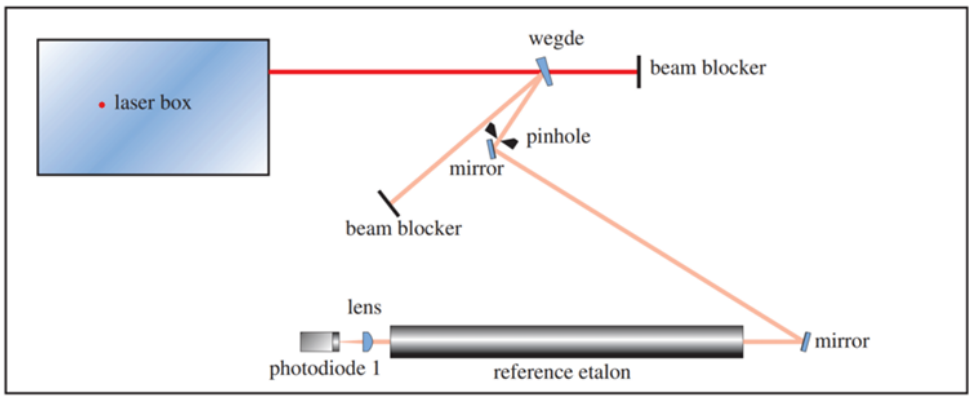

Figure 4: Optical setup for measuring FPI transmission curves. Attenuator used was T=0.105[1]

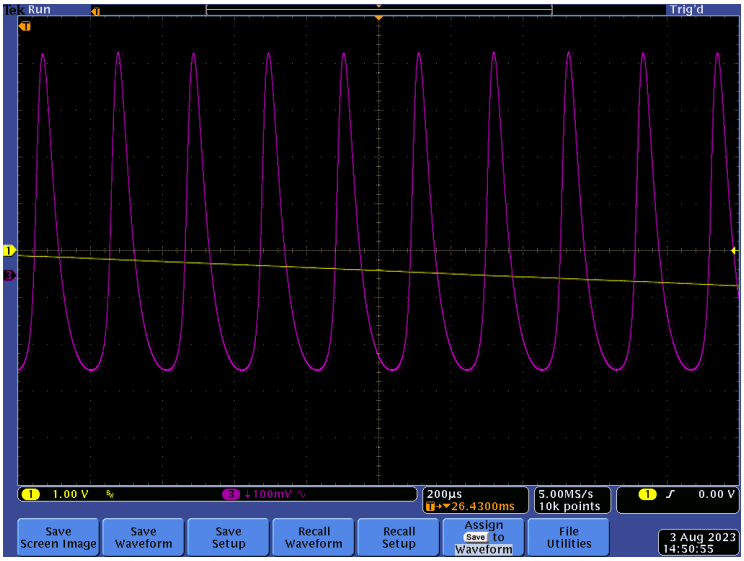

Figure 5: Oscilloscope window showing transmission curves of Farby Perot cavity of length 500mm along the falling ramp of the sawtooth signal

2.2.2 Analysis of Transmission Curves of FPI

As seen in Fig(6) the transmission curves are quite asymmetric about their centre.So the signal containing transmission curves from the FPI (Fig(8)) was fitted using asymmetric Lorentzian function.[2] This asymmetry can be caused by difference in coupling between the two mirrors, i.e a path difference in the on-axis and off-axis beam.[3]. From the asymmetric

[2]See Appendix

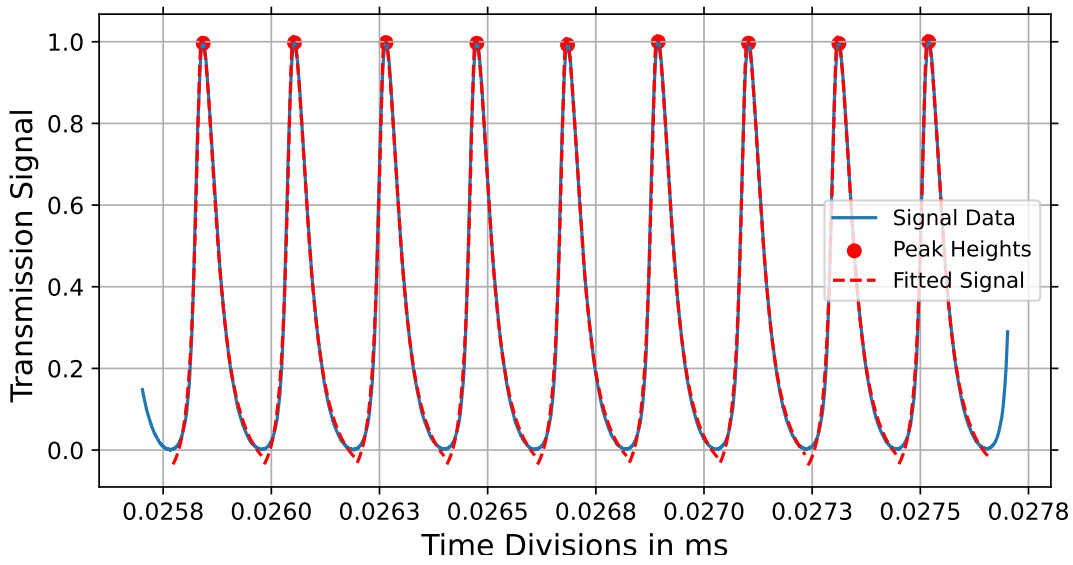

Figure 6: Uncalibrated Transmission Curve signal. The data was normalised and the time divisions were subtracted to get only time difference

Lorentzian fit used for the transmission curves in Fig(8),-

- Average $\Delta\nu_{mode}$=0.20965±21e-12 ms
- Average $\Delta\nu_{FWHM}$ = 0.0583465 ± 2e-11 ms

The calibration factor is obtained by $\Delta\nu_{modecalib}$

$$\textbf{calib factor} = \frac{\Delta\nu_{modecalib}}{\Delta\nu_{mode}} = \frac{149.9348}{0.20965}\text{GHz/s} = \textbf{715.16718 GHz/s} \tag{10}$$

Further Finesse of the FPI can be calculated . Using the factor in Eq(10)

$$\mathcal{F} = \frac{2\Delta\nu_{mode}}{\Delta\nu_{FWHM}} = \textbf{7.186} \tag{11}$$

which differs from the predicted value of the Finesse .This maybe due to losses, change in mode spacing overtime and non-optimal coupling.

- Average $\boldsymbol{\Delta\nu_{\mathbf{mode}} = 149.9348 \pm 2e-9}$ Mhz
- Average $\boldsymbol{\Delta\nu_{\mathbf{FWHM}} = 41.727 \pm 1e-8}$ MHz

The mode spacing of the transmission curves decreases with increase in time/frequency as seen in Fig(7).This implies an increase in scanning frequency towards the end i.e laser scanning rate is not constant.Ideally,this requires the calibration process to take into account the actual mode spacing over a range, so that the calibrated frequency can be expressed as

$$\Delta\nu = \frac{\Delta t}{\Delta t_{mode}} \Delta\nu_{average/calibrated} \tag{12}$$

As this deviation is in the order of 0.5 for this data, an average value is taken for calibration of the data presented hereafter. So using an average calibration, the calibrated transmission

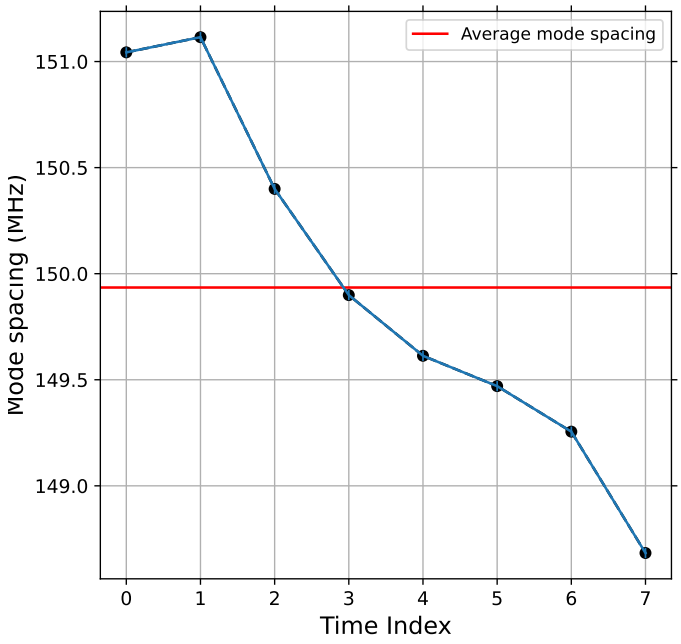

Figure 7: The mode spacing was plotted vs the index of time scales simulating an increase in time difference

curves are as seen in Fig(8)

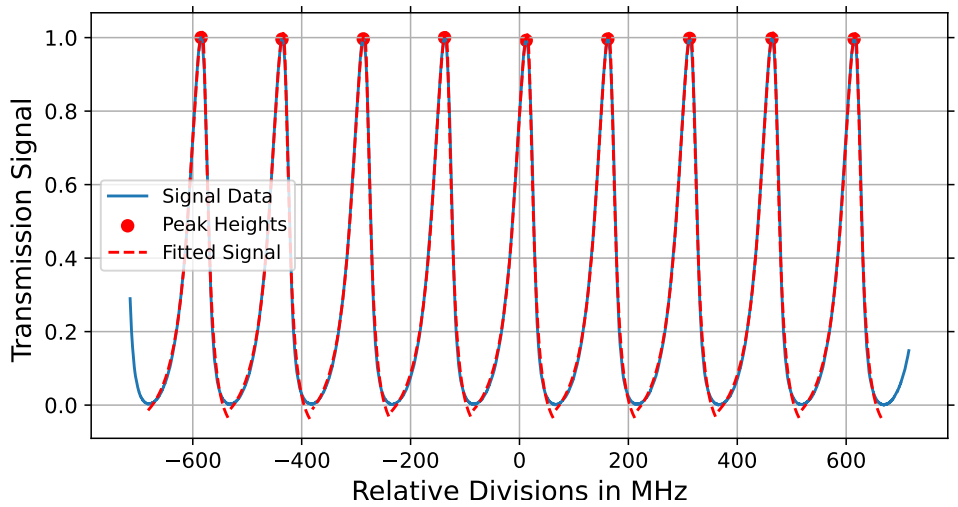

Figure 8: Calibrated Transmission curves over the range of 1.2GHz.These curves wer calibrated using the mode spacing 149.9348±2e-9 Mhz

2.3 Linear Spectroscopy

2.3.1 Theoretical Predictions of Rubidium Spectrum

At $\lambda = 794$ nm , Rubidium D1 lines can be accessed. There is a splitting between energy levels of ground and excited sttae due to hyperfine interactions of nuclear and electronic state.To calculate the possible transitions, the various quantum numbers need to be considered.The total angular momentum $\vec{F} = \vec{J} + \vec{I}$.The selection rules are $\Delta F, \Delta J = 0, \pm 1$[4] For both $5P_{1/2}$ and $5S_{1/2}$ levels, the value of the electronic spin J is $J = \frac{1}{2}$.The nuclear spin values for ^{85}Rb is $I = \frac{5}{2}$ and for ^{87}Rb, $I = \frac{3}{2}$. [5, 6] The range of values for the total spin F lies between:

$$|I - J| \leq F \leq I + J \tag{13}$$

Given the values of I and J, for ^{85}Rb, $F = 2$ and $F = 3$ and for ^{87}Rb, $F = 1$ and $F = 2$.Thus according to specific selection rules the possible transitions are listed in Fig(9)

From [5, 6], the energy level diagram for a mixture of Rb_{87} and Rb_{85} is calculated theoretically, to predict the energy of each transition, given in Table(1). The isotope shift can be calculated as the difference in excited state energy levels of the two isotope.From the values in[5, 6]

$$\Delta E_{\text{isotope}} = h.77.583(12)MHz \tag{14}$$

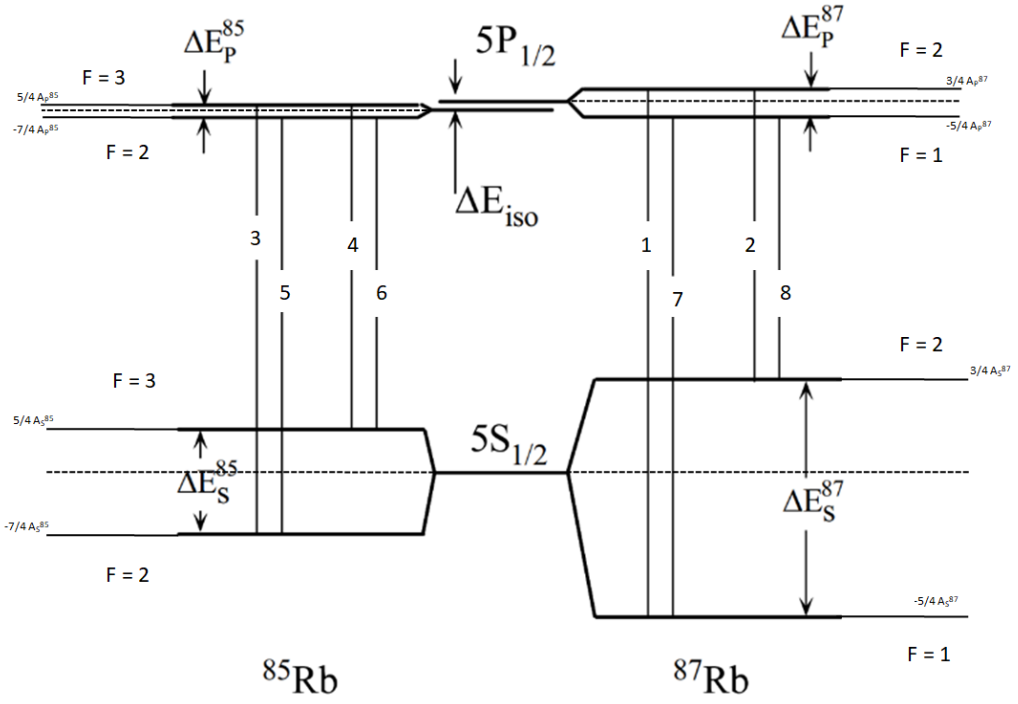

Figure 9: Energy Transitions possible for Rb85 and Rb87 D1 lines. The lines are numbered according to increase in transition Energy

	F → F'	**S → P (THz)**	**Hyperfine Transition offset (THz)**	**Hyperfine Transition (THz)**
1	87:2-1	377.1074635	-0.00307341597	377.1043901
2	87:2-2	377.1074635	-0.002253813	377.1052097
3	85:3-2	377.1072856	-0.001475811	377.1058098
4	85:3-3	377.1072856	-0.0014155441	377.1058701
5	85:2-2	377.1072856	0.001559920022	377.1088455
6	85:2-3	377.1072856	0.001921502922	377.1092071
7	87:1-1	377.1074635	0.0037612666	377.1112248
8	87:1-2	377.1074635	0.0045779226	377.1120414

Table 1: Hyperfine energy transition lines of Rubdidum D1 transitions.The lines are arranged in increasing order of frequency.The lines are measured according to the lowest transition ie Rb 87 F=1 to F'=1

Predicted FWHM values

Due to thermal velocity of atoms, the Voigt lineshape of the absorption spectra is transformed to a Doppler broadened peak[1]. The Doppler width can be calculated as -

$$\Delta\nu_{\text{Doppler}} = \nu_o\sqrt{\frac{kT}{m_{\text{atom}}c^2}} \tag{15}$$

For the values

- T(room temperature) $\approx 300K$
- $m_{Rb85} = 1.40999 \times 10^{25}$ kg (mass of the atom)
- $m_{Rb87} = 1.44316 \times 10^{25}$ kg
- $\nu_{o,i} = 377.1074635$+(ith line frequency offset) THz

The typical $\Delta\nu_{\text{Doppler}}$ was found to be $\approx 0.5GHz$.Though this is not the true FWHM of the transition curves, as the voigt lineshape would also contribute to this FWHM.[1, 5, 6]

Hyperfine Splitting Constant and energy Difference

The hyperfine energy split can be written as[5, 1, 6]:

$$\Delta E_{HFS} = \frac{1}{2}\cdot A_{HFS}(I,J,F)\cdot[F(F+1) - I(I+1) - J(J+1)] \tag{16}$$

Substituting the values of F, I and J for ^{85}Rb and ^{87}Rb respectively,

$$\Delta E_{HFS} = 3\cdot A_{HFS,85} \tag{17}$$

$$\Delta E_{HFS} = 2\cdot A_{HFS,87} \tag{18}$$

The theoretical values of the transition are then given by Table(2)

Hyperfine Constant	**Energy Value**
$A_{85S_{1/2}}$	h · 1011.910 MHz
$A_{85P_{1/2}}$	h · 120.527 MHz
$A_{87S_{1/2}}$	h · 3417. 341 MHz
$A_{87P_{1/2}}$	h · 408.328 MHz

Table 2: Theoretical Values of Hyperfine Splitting Constants Taken from[5, 6]

Thus from the theoretical peak values, approximate FWHM and the intensities derived from the transition probabilities[1], the spectral profile can be predicted and is plotted in Fig(10)

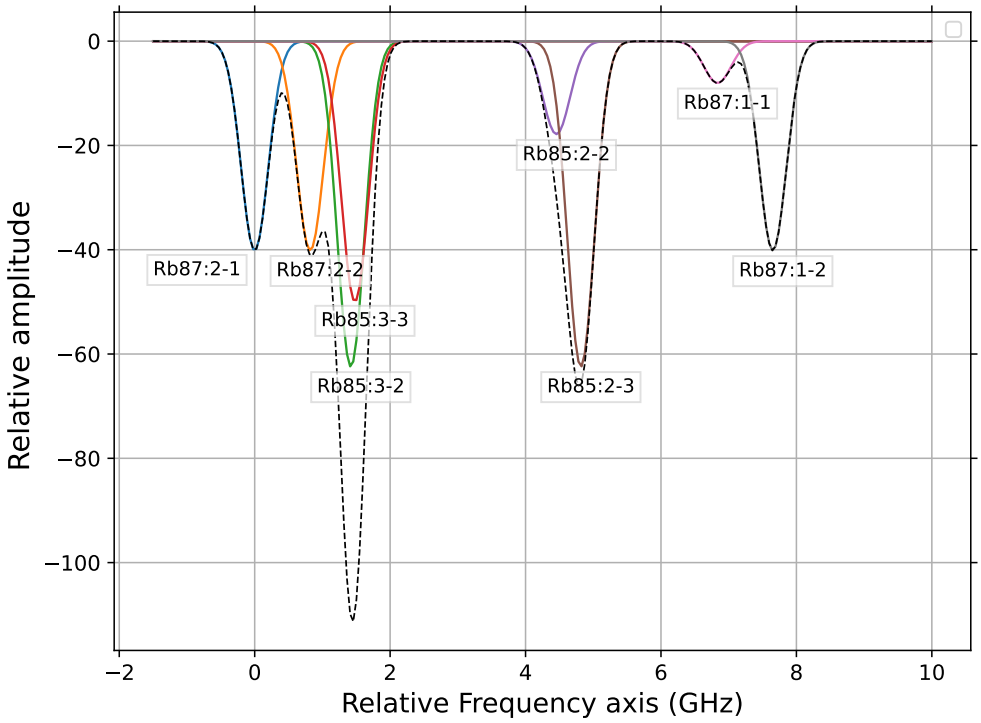

Figure 10: Theoretical Prediction of the Rb D1 lines. A multi gaussian curve with an offset with the predicted peak centres, FWHM and intensities was modelled to plot this curve.

2.3.2 Experimental Setup

In this setup linear spectroscopy of Rubidium spectrum is done using the scanning laser. The Rubidium sample used is a natural mixture of Rb_{85} and Rb_{87}.The injection current of the laser is set to **162 ± 0.5 mA**, which is equivalent to an $P_{avg} = 66.116mW$(calculated from Fig(3). But here two attenuators of $T = 0.105, 0.37$were used and power was attenuated to **0.2568 mW**. The setup was done as shown in Fig(11) with a 5cm long cell filled with Rubidium Vapour at room temperature. The data from the photodiode was read off through the oscilloscope. In the second part of this experiment, the spectrum was recorded

for 2cm cell, 5cm cell and the combined cell length of two previous cell 7cm cell.

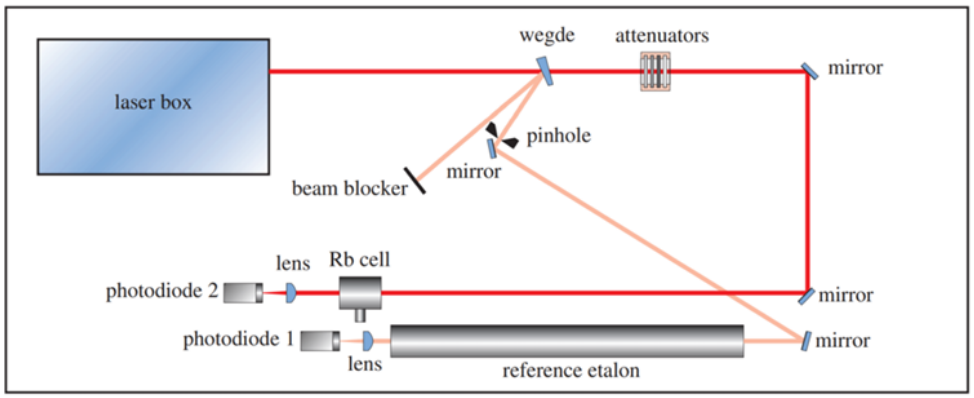

Figure 11: Optical Setup for Linear Spectroscopy of the natural mix of Rubidium Istopes 85 and 87

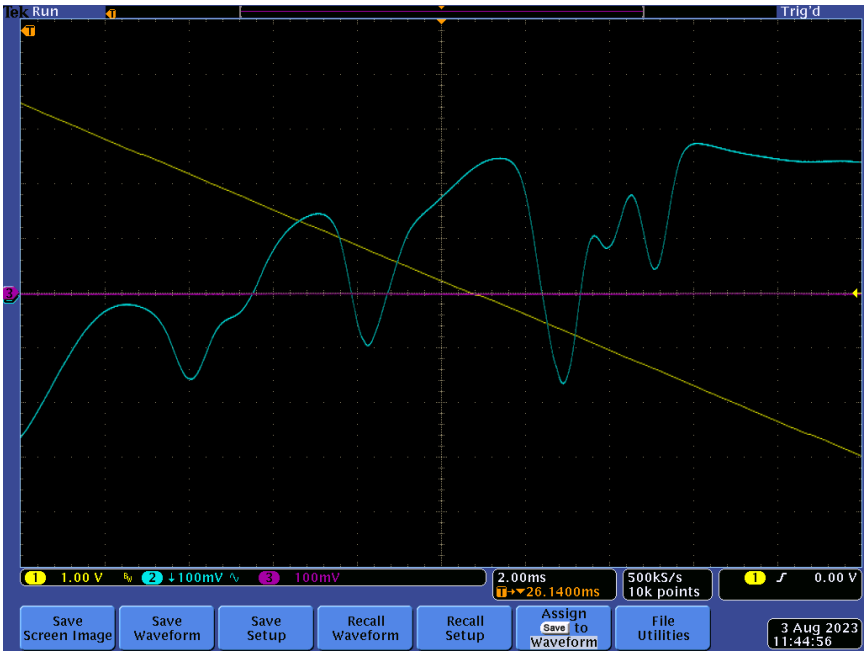

Figure 12: Oscillation window showing transition curves of Rubidium Spectrum along the falling ramp of saw tooth signal

2.3.3 Analysis

As seen from Fig(12), the spectrum is along the falling ramp of the saw tooth and has an additional linear background.After inverting, normalising and subtracting a linear background, the spectrum was fitted with individual Gaussian curves centred around each peak.Except lines 3 and 4 (ass given in Fig(insert that energy diag)) the other peaks were fitted with individual gaussian. The fitting of the curve is not optimised as the calibration is done based on an average mode spacing.The amplitude, centre of peak and width(σ) were calculated from the fit.The FWHM was calculated using

$$\Delta\nu_{FWHM} = 2\sqrt{2ln2}\sigma \approx= 2.355\sigma \tag{19}$$

The relative intensity is calculated from the approximate formulae

$$I = \sqrt{(}2\pi)A\sigma \tag{20}$$

The resolution of individual peak were calculated based on the wavelength $\lambda = 794$ nm or$\nu_o = 377.833$THz-

$$\frac{\Delta\nu}{\nu_o} = \frac{\Delta\nu_{FWHM}(GHz)}{377.833(THz)} \tag{21}$$

line	$\Delta\nu$ **GHz**	$\Delta\nu$ **Error**	σ **GHz**	σ **error GHz**	**Relative Amplitude(A)**	**Relative intensity(I)**	**FWHM GHz**	**FWHM error**	**Resolution** 10^{-6}	**Resolution error**
1	2.49000	0.000740	0.2315	0.03102	90.60717	52.57192	0.54512	0.073052	1.442751	0.13401
2	4.59806	0.000000	0.1422	0.02968	182.4085	65.02332	0.334908	0.069894	0.886389	0.208697
3+4	4.37000	0.000610	0.3222	0.020962	182.4085	147.3137	0.758751	0.049366	2.00816	0.065062
5	6.83000	0.000020	0.4450	0.01730	97.2268	108.4516	1.047975	0.040733	2.773641	0.038869
6	8.39000	0.000060	0.1441	0.00972	92.20223	33.31201	0.339438	0.02289	0.898379	0.067435
7	9.41000	0.000030	0.3177	0.00581	90.20875	71.84943	0.7483	0.013678	1.9805	0.018279
8	11.00000	0.000010	0.2005	0.03552	92.51898	46.48864	0.472082	0.08364	1.249442	0.177172

Table 3: Spectrum Parameters from individual Gaussian fit.Line3 and 4 corresponding to Rb 85 could not be resolved

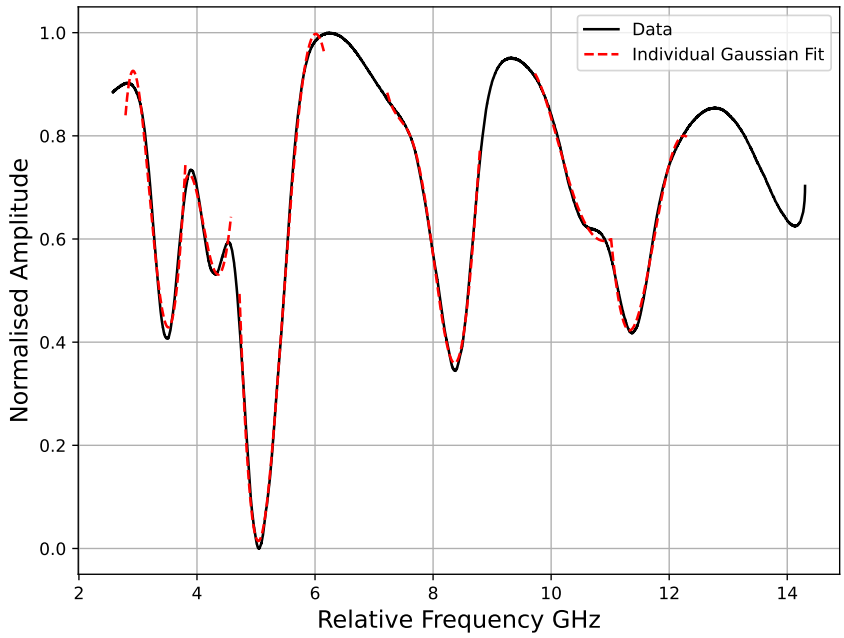

Figure 13: Rubidium Spectrum curves fitted with individual gaussian.The spectrum ranges over approximately 12 Ghz

FWHM and Doppler width of peaks

The Doppler width of the peaks calculated from Eq(15) are

- Rb_{85}=502.01 MHz
- Rb_{87}=497.23 Mhz

Considering the most isolated line of Rb_{87} ,line 1, $\mathbf{\Delta\nu_{1FWHM} = 0.542Ghz \pm 0.073}$. And similarly considering the most isolated line of Rb_{85}, line 8, $\mathbf{\Delta\nu_{8FWHM} = 0.4720Ghz \pm 0.0834}$. This difference as previously stated is caused due to Voigt lineshape, which also contributes to the spectral profile and not considered in this calculation. [1]

Resolution of Peaks

Th resolution of most isolated peak line 1 is given by $\mathbf{(1.442751 \pm 0.13401) \times 10^{-6}}$. Though this is an appropriate resolving power for Rb_{87} lines, Rb_{85} were not mostly resolved.

Hyperfine Splitting Constants from Linear Spectroscopy

For the fit on Rb spectrum only one 85 line was not properly resolved. So with each hyperfine constant two lines are associated. Experimentally the constant is calculated by , taking the average of to such transition

- $A_{85S_{1/2}} = h\frac{\Delta\nu_7 - \Delta\nu_2}{2} = h\frac{\Delta\nu_8 - \Delta nu_1}{2} = \mathbf{h.3.33 \pm 0.0106}$ GHz
- $A_{87P_{1/2}} = h\frac{\Delta\nu_8 - \Delta\nu_7}{2} = h\frac{\Delta nu_2 - \Delta nu_1}{2} = \mathbf{h.0.924 \pm 0.0115}$ GHz
- $A_{85S_{1/2}} = h\frac{\Delta\nu_5 - \Delta\nu_{3+4}}{3} = h\frac{\Delta nu_6 - \Delta nu_{3+4}}{3} = \mathbf{h.1.08 \pm 0.0119}$ Ghz
- $A_{85P_{1/2}} = h\frac{\Delta nu_5 - \Delta nu_6}{3} = \mathbf{h.0.52 \pm 0.0065}$ Ghz

Comparing the theoretical values given in Table(1)$A_{85P_{1/2}}$ and $A_{87P_{1/2}}$ deviates largely from its theoretical value. The deviation for $A_{85P_{1/2}}$ maybe caused due to non-optimised fitting as seen in Fig(13), due to the low spectral resolution of the curve.$A_{87P_{1/2}}$ value deviation maybe explained by the error in calibration caused by an average mode spacing, leading to large differences in curves placed far away on frequency scale.

Verifying Beer Lambert's Law

Beer Lambert's law gives the relationship between absorption and optical length. From this law, it can be implied that intensity and cell length will have a linear relationship.[1]

$$A \propto l$$

Th transmission curves of three different Rubidium Cell were considered(Fig(14)) From Fig(14) , it can be qualitatively concluded that the depth of the peaks and thus intensity increases with increase in cell length. Considering line 1 as it is the most isolated resolvable peak in the spectrum, gaussian fitting is done to calculate the parameters.

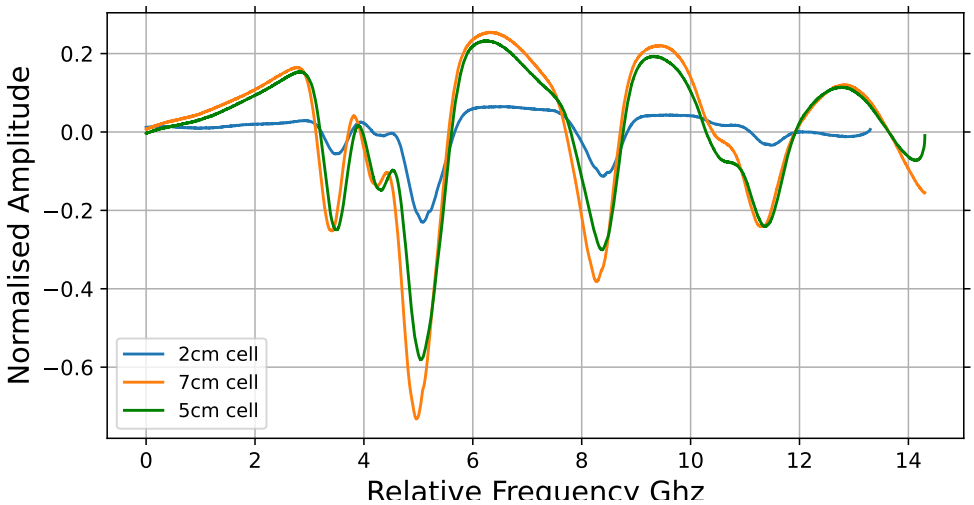

Figure 14: Rubidium Transition curves for different length of Rubidium Vapour cell

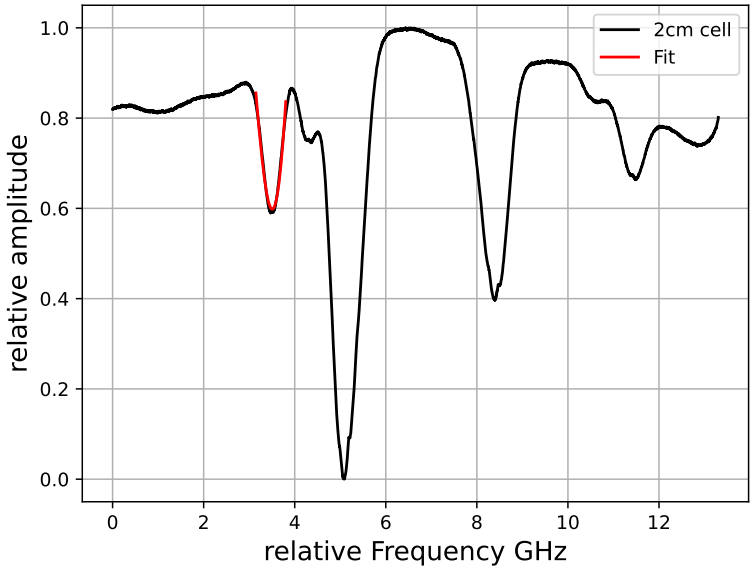

Figure 15: Normalised Rubidium spectrum for a 2cm cell

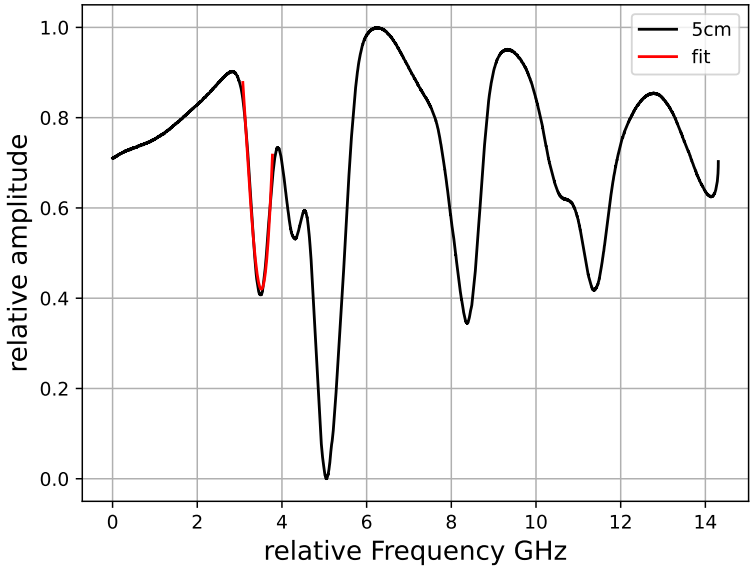

Figure 16: Normalised Rubidium spectrum for a 5cm cell

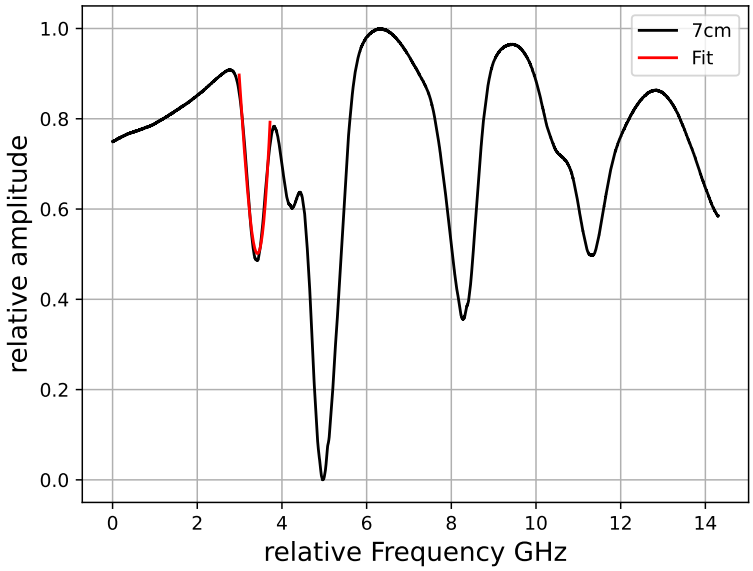

Figure 17: Normalised Rubidium spectrum for a 7cm cell

The relative intensity is then plotted against the cell length. An almost linear model can be fitted to the curve in Fig(18) inspite of large errors. Thus Beer Lambert law can be

verified from here.

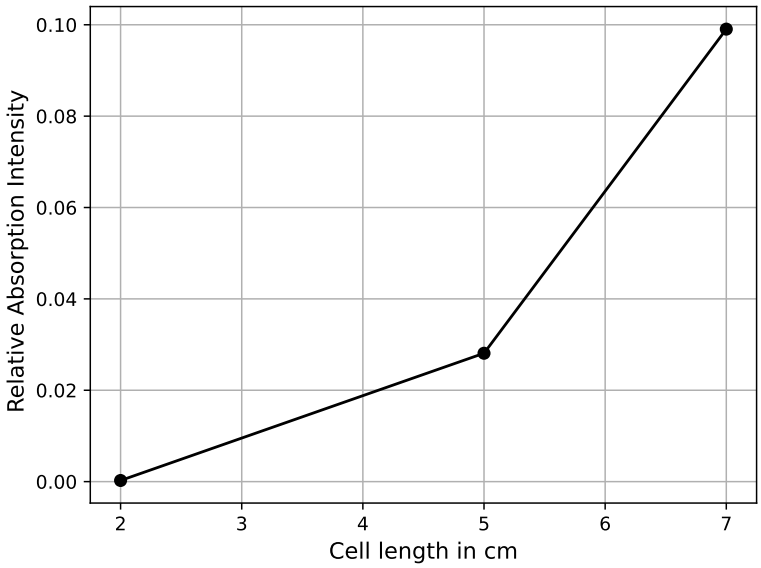

Figure 18: Relative Intensities plotted against the cell length used

2.4 Non-linear Spectroscopy

This section discusses the nonlinear spectroscopic technique used to obtain the saturated absorption spectrum.

2.4.1 Theoretical Aspects of Non-linear Spectroscopy

The experiment is conducted with two counter propagating beams one of high intensity and one less intense, with the same frequency.the transition spectrum obtained is saturated by the strong pump beam, but the weak probe beam helps in burning holes in the spectra ,as a consequence of which lamb peaks and cross-over peaks are observed. Crossover peaks are further resonances when in the same Doppler profile , one transition is blue-shifted and the other transition is redshifted. This leads to resonances in absorption , dealing with different velocity class and positioned at the centre of the two frequencies. [7].The predicted crossover resonances are thus listed

Transition Scheme	**Transition Energy (THz)**
87:2→ 1	377.1043901
87:2→ CO12	377.1047999
87:2→ 2	377.1052097
85:3→ 2	377.1058098
85:3→ CO23	377.1058399
85:3→ 3	377.1058701
85:2→ 2	377.1088455
85:2→ CO23	377.1090263
85:2→ 3	377.1092071
87:1→ 1	377.1112248
87:1→ CO12	377.1116331
87:1→ 2	377.1120414

Table 4: Predicted transition in the saturated spectrum of Rubidium, probed by a weak beam.87:2→ CO12 and 87:1→ CO12 are not seen as the interacting transitions are not in the same Doppler profile.

2.4.2 Experimental Setup

The experimental setup is the same as that in the previous linear spectroscopy case (see figure 19), with the beam blocker removed and instead, attenuators were placed for

the strong beam to pass through into the Rb cell and an additional photodiode for measurement. The 5cm Rb cell is used and the Lamb-peaks in the spectra are observed and hyperfine constants, resolution and isotope shift are calculated. The saturation power and intensity are also determined, varying the attenuation.The entire experiment was conducted with a fixed attenuation of T=0.105.

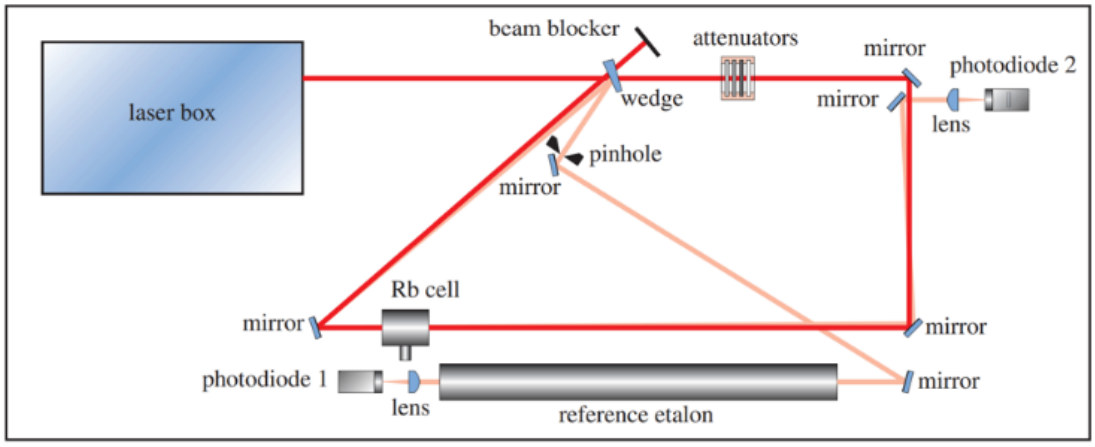

Figure 19: Experimental setup for non-linear spectroscopy [1]

2.4.3 Measurement and Analysis

Spectral Analysis

Various combinations of attenuators were used and the spectra for each were obtained. From the spectra, the baseline modelled by a polynomial was subtracted. The time-calibrated conversion factor obtained from the FPI was applied.

The best-resolved lamb peaks were seen for the attenuator valued at $T = 0.512$. In the obtained spectra, transitions numbered 8, 7, 6 and 5 each are represented by a Lamb peak and transitions 4 and 3, along with 2 and 1 have overlaps, so they have a cross-over peak between the lamb peaks.

To analyze the peaks and extract values from them, asymmetric Lorentzian fits are applied individually, as expected from the theory due to the absence of Doppler effects, unlike the Gaussian shapes obtained in the linear case.

The fit obtained is seen in Figure(20). The parameters obtained from the fits are in Table(5).

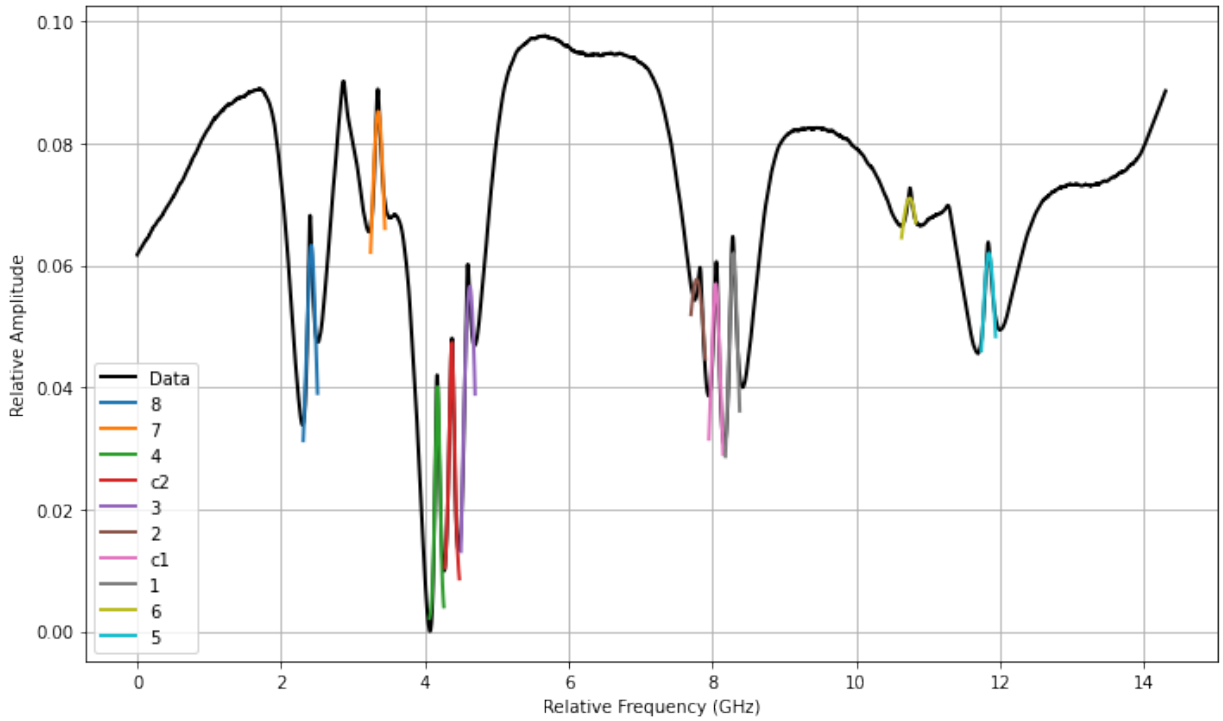

Figure 20: Non-linear absorption spectrum with Lorentzian fits for Lamb peaks and cross-over resonances

For the fits for peaks 3 and 2, the uncertainties could not be determined. This could be because of the statistics involved in the fitting or because of the nature of the data.

Peak	**Center (GHz)**	**FWHM (GHz)**	**Relative Amplitude**	**Resolution 10^{-5}**
8	2.42029084 +/- 0.00107501	0.22150168 +/- 3.38726	0.0272327227 +/- 1.41671323	0.0586242 ±3.387
7	3.35095570 +/- 8.0024e-04	0.34627244 ±1.447615887	0.02467227766 +/- 5.22805406	0.091647 ±1.4476158
4	4.17619193 +/- 5.5150e-04	0.08704604 ±0.012005	0.06124309 +/- 1.728503	0.0230382 ±0.012005
C2	4.37447824 +/- 2.7709e-04	0.099481324 ±0.98522	0.0536632256 +/- 4.79214516	0.0263294 ±0.98522
3	4.62427048	0.100826103	0.012305	0.0266853
2	7.77972315	0.3537436756	0.023346	0.0936243
C1	8.04560445 +/- 7.9882e-04	0.21046044 ±2.35079742	0.02433455795 +/- 5.84480981	0.0557019 ±2.35079742
1	8.29148197 +/- 6.3237e-04	0.20688312 ±2.8501267	0.02420629835 +/- 3.11650322	0.054755 ±2.8501267
6	10.7427960 +/- 0.00157603	0.71408586 ±3.380218	0.161553317 +/- 1.35953506	0.188995 ±3.380218
5	11.8446827 +/- 6.6068e-04	0.35514162 ±7.17568	0.01305388830 +/- 2.40195808	0.093994 ±7.17568

Table 5: Parameters of the Lorentzian fit for each peak

Hyperfine Coupling constants

The hyperfine coupling constants are calculated with the center frequency of the different lamb peaks. The energy of the splittings can be expressed as $\Delta E = h \cdot \Delta\nu$ and this is used to calculate the hyperfine coupling constants.

Energy Shift	**Center Frequency difference (GHz)**	ΔE **(h.GHz)**	A_{HFS} **(h.GHz)**
ΔE_S^{87}	$\nu_7 - \nu_5$	8.493727 ± 0.0001	4.2468635 ± 0.00005
ΔE_S^{87}	$\nu_8 - \nu_6$	8.3218876 ± 0.0005	4.1609438 ± 0.00025
ΔE_P^{87}	$\nu_6 - \nu_5$	1.1018867 ± 0.0009	0.55094335 ± 0.00045
ΔE_P^{87}	$\nu_8 - \nu_7$	0.93066486 ± 0.0002	0.46533243 ± 0.0001
ΔE_S^{85}	$\nu_4 - \nu_1$	4.11469004 ± 0.0008	1.3715633466 ± 0.00027
ΔE_S^{85}	$\nu_3 - \nu_2$	3.15546102	1.05182034
ΔE_P^{85}	$\nu_2 - \nu_1$	0.51175882 ± 0.0006	0.17058627 ± 0.0002
ΔE_P^{85}	$\nu_4 - \nu_3$	0.45007855 ± 0.00056	0.1500261833 ± 0.00012

Table 6: Energy shifts and their corresponding frequency differences and hyperfine constants

In table 5, the energy is calculated from the central frequencies and then the hyperfine constants are calculated from the energy based on equations 17 and 18. The average of the values are taken for the possible frequency differences that correspond to specific hyperfine splittings and the hyperfine constants are calculated as:

$$A_{85}^{avg}(^5S_{1/2}) = 1.2135 \pm 0.00015GHz \tag{22}$$

$$A_{85}^{avg}(^5P_{1/2}) = 0.1603 \pm 0.00022GHz \tag{23}$$

$$A_{87}^{avg}(^5S_{1/2}) = 4.2039 \pm 0.000015GHz \tag{24}$$

$$A_{87}^{avg}(^5P_{1/2}) = 0.5081 \pm 0.00023GHz \tag{25}$$

The theoretical values are mentioned in Table 2 and the calculated values are close but are seen to deviate from them possibly because of the fitting with the asymmetric Lorenztian and from the conversion factor obtained from the calibration. Moreover, errors from the oscilloscope or from time gauging were not considered.

Spectral Resolution

The spectral resolution is calculated from the FWHM of the peaks.

$$R = \frac{\Delta\nu}{\nu_0} = \frac{\nu_{FWHM}(GHz)}{377.833(THz)} \tag{26}$$

The resolution obtained for the individual peaks is mentioned in Table(5).

Isotope Shift

The hyperfine energy split is calculated as [1]

$$\Delta E_{HFS} = \frac{1}{2} \cdot A_{HFS}[F(F+1) - I(I+1) - J(J+1)] \tag{27}$$

And the isotope shift is calculated by

$$\Delta E_{iso} = h \cdot [(\nu_5 - \nu_1) - \frac{3}{8}(\nu_5 - \nu_6) - \frac{5}{8}(\nu_5 - \nu_7) + \frac{5}{12}(\nu_1 - \nu_2) + \frac{7}{12}(\nu_1 - \nu_3)] \tag{28}$$

The frequency differences can be written in terms of the calculated hyperfine coupling constants. The isotope shift is calculated as:

$$\Delta E_{iso} = \mathbf{h} \cdot (\mathbf{0.235 \pm 0.875})\mathbf{GHz} \tag{29}$$

Within the error range, this complies with the theory in Eq(14). Possible sources of error are most likely from the statistics of the fit, the relative error due to the addition of various results and due to the averaged mode spacing value for calibration.

Saturation Power

The rate at which the saturation of a transition of the medium occurs is given by the saturation parameter [1]

$$S = \frac{P}{P_{sat}} \tag{30}$$

where P_{sat} is the saturation power. The effect of saturation on the Lamb peaks can be seen through its intensity, as the intensity also saturates by

$$I(P) \propto \frac{S}{S+1} = \frac{1}{1 + \frac{P}{P_{sat}}} \tag{31}$$

The lamb peak also broadens with increasing laser power by

$$\Gamma(P) = \Gamma_0\sqrt{1+S} = \Gamma_0\sqrt{1 + \frac{P}{P_{sat}}} \tag{32}$$

where Γ is the absorption profile and Γ_o is the natural linewidth. The theoretical Value of the natural linewidth is given by $\mathbf{2}\pi \times \mathbf{6.065(9)MHz} \approx \mathbf{38MHz}$[5] This can be observed

experimentally by the use of different attenuators to vary the beam power P. The fit analysis was done for one peak for all the different values of attenuations (Table (7)).

Attenuation T	**Center (GHz)**	**Pump Power**	**Relative Amplitude**	**FWHM (GHZ)**
0.006	-	104946.0317	-	-
0.019	2.46870763 +/- 0.01585898	33140.8521	8.17268178	0.48261721 +/- 1.98519022
0.037	2.45766717 +/- 0.00712394	17018.2754	7.15950765	0.30509909 +/- 0.43094679
0.164	2.44907933 +/- 346.239022	3839.4889	0.05463059	0.23777905 ±2.0493
0.321	2.44394231 +/- 0.00129559	1961.6080	0.477103978	0.22545632 ±0.031908
0.512	2.42029084 ±0.00107501	1229.8363	0.272327227	0.22085866 ±0.034128
1	$2.43198926 \pm 9.1073e-04$	629.676	1.05731373	0.2143877 ±0.021402

Table 7: Parameters of the fit for different values of attenuation

To obtain the pump power, the average in the linear spectroscopy section was used and corrected with the appropriate values of attenuation (the fixed one in front of the laser and the additional ones). For the lowest attenuation value, due to the resolution of the peaks, the fit was not obtained and hence the parameters could not be determined. Moreover, the errors could not be calculated for the amplitude and hence this affected our results significantly.

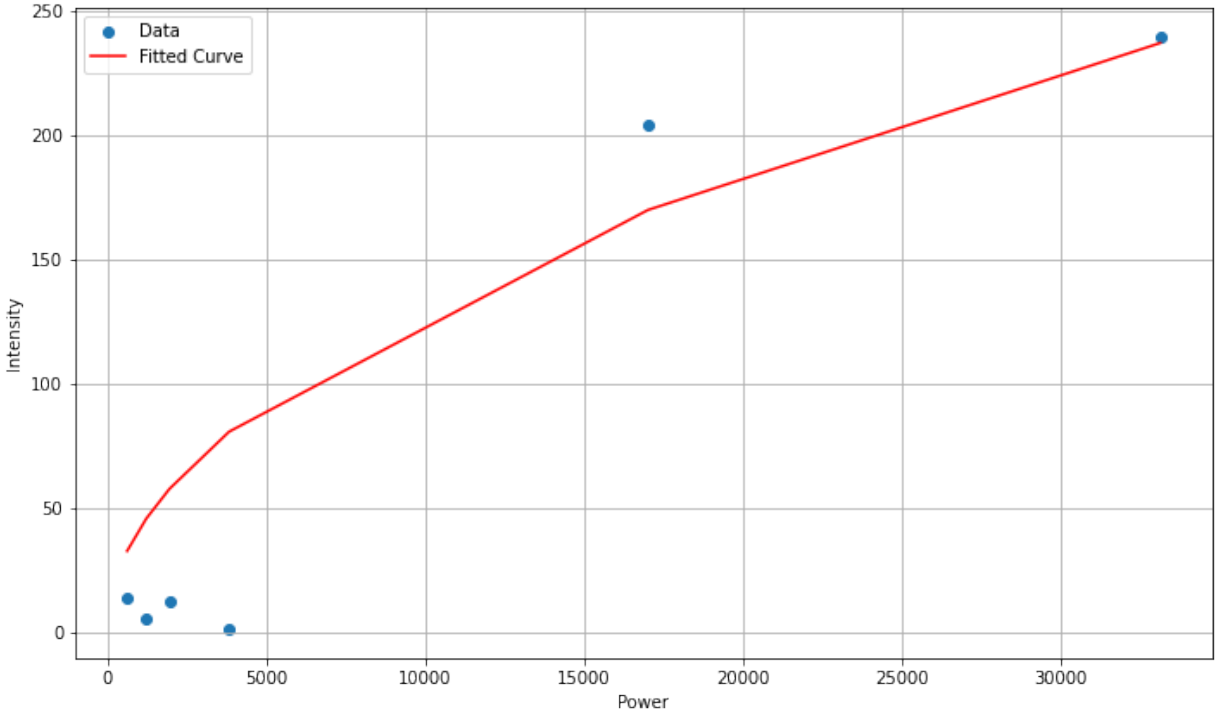

Figure 21: Caption

From the fits, the intensity of the peaks was calculated and plotted against the non-attenuated pump power in Fig(21). This plot was then fitted using the function in Eq(32). From this fit the saturation power $\mathbf{P_{sat}} = (0.75 \pm 4.48)mW$ The saturation intensity theoretically is given by the formulae[5]

$$I_{sat} = \frac{\hbar\omega^3\Gamma_o}{12\pi c^2}$$

Considering the typical values for

- $\nu = 377.83 \times 10^{12}$Hz
- $\Gamma_o = 38 \times 10^6$s
- speed of light in air $c = 3 \times 10^8 ms^{-1}$

The theoretical saturation intensity was calculated as $\mathbf{I_{sat} = 93.70 Wm^{-2}}$ Experimental saturation intensity is calculated using the formula

$$I_{sat} = \frac{P_{sat}}{\text{Cross sectional area of beam}} = \frac{P_{sat}}{\pi r^2} = (106.103 \pm 5.704)Wm^{-2} \qquad (33)$$

where r is the laser beam diameter taken as $\mathbf{1.5 \pm 0.5 mm}$

3 Conclusion

1. Diode Laser Characteristic was obtained . A relationship between output power and injection current was established.$I_{threshold}$ and quantum efficiency of the laser was deterimined.

2. The FPI transmission curves were utilised to calibrate the time division. The mode spacing showed a decreasing trend with increase in time spacing but a average mode spacing was adopted for calibration.

3. Linear spectroscopy of Rubidium was performed and the spectra was analysed.The Rb 85 transitions was not resolved properly in this fit and this led to further errors in the analysis. Hyper splitting constants, Doppler width and resolution of the peaks were calculated and compared with the theoretical values. The Rubidium Spectrum was analysed using three different cell of length 2cm, 5cm and 7cm. Beer-Lambert law was found to be satisfied (with large errors) from relative intensity vs optical length plot

4. Non-linear spectroscopy of Rubidium was performed to obtain saturated absorption spectra. The lamb peaks and crossovers were observed and a Lorentzian fit was applied to the spectra. The parameters from the fit were used to obtain the hyperfine coupling constants with higher accuracy. The resolution and isotope shift were also calculated. The fit performed led to a lot of errors owing to its statistics and in some cases uncertainties were not determined. The first peak corresponding to $5S_{1/2}(F = 2) \rightarrow 5P_{1/2}(F' = 1)$ for different attenuations were also plotted and fits were made and from this the saturation power and intensity were determined. The fits could not be performed well, and uncertainties could not be determined, particularly for lower values of attenuation and this affected the calculated values.

Areas to Optimize Setup and Analysis

The primary error that arises in this analysis is from calibration. As the mode spacing of transmission curves from FPI decreased with time scale, the calibration factor used for the analysis should have been based on such an function decreasing with time scale, interpolated from the mode spacing data. Further experimentally to reduce such trend in mode

spacing, better in coupling to the FPI is required.This can been done by repeated laser beam walking. The laser scanning could have been further tuned to be more continuous by varying the laser temperature , injection current and scan frequency.
Further the background of the rubidium spectrum is not perfectly linear. This again rises from skewed propagation of laser beam into the rubidium cell, leading to reflections from the cell wall.

4 Appendix

Laser Characteristics fit

The laser Power vs Current was fited according to the linear

$$P(I)mA = 0.4081 \pm 0.000013ImA + -19.48 \pm 0.0695$$

Aymmetric Lorentzian Function

$$f(x; A, \mu, \sigma, \sigma_r) = \frac{2A}{\pi(\sigma + \sigma_r)}\Big[\frac{\sigma^2}{(x-\mu)^2 + \sigma^2} * H(\mu - x) + \frac{\sigma_r^2}{(x-\mu)^2 + \sigma_r^2} * H(x - \mu)\Big]$$

where H is the heavyside function.FWHM of such Lorentzian is calculated by summing up the two widths ie. $\sigma + \sigma_r$

References

[1] *A246-HighResolutionLaser Spectroscopy*. English. University of Bonn, Physics Department.

[2] Wolfgang Demtröder. *Laser spectroscopy: vol. 2: experimental techniques*. Vol. 2. Springer Science & Business Media, 2008.

[3] Michael Hercher. "The Spherical Mirror Fabry-Perot Interferometer". In: *Appl. Opt.* 7.5 (May 1968), pp. 951–966. DOI: 10.1364/AO.7.000951. URL: https://opg.optica.org/ao/abstract.cfm?URI=ao-7-5-951.

[4] C.J. Foot. *Atomic Physics*. Oxford Master Series in Physics. OUP Oxford, 2005. ISBN: 9780198506959. URL: https://books.google.de/books?id=%5C_CoSDAAAQBAJ.

[5] Daniel Steck. "Rubidium 87 D Line Data". In: 2003. URL: https://api.semanticscholar.org/CorpusID:122524490.

[6] Daniel Steck. "Rubidium 85 D Line Data". In: 2008. URL: t%20http://steck.us/alkalidata%20(revision%202.2.3,%209%20July%202021).

[7] Daryl W. Preston. "Doppler-free saturated absorption: Laser spectroscopy". In: *American Journal of Physics* 64.11 (Nov. 1996), pp. 1432–1436. ISSN: 0002-9505. DOI: 10.1119/1.18457. eprint: https://pubs.aip.org/aapt/ajp/article-pdf/64/11/1432/11979448/1432_1_online.pdf. URL: https://doi.org/10.1119/1.18457.